Research article

Journal of MASS SPECTROMETRY

Received: 19 August 2013 Revised: 21 November 2013 Accepted: 21 November 2013 Published online in Wiley Online Library

(wileyonlinelibrary.com) DOI 10.1002/jms.3317

Mechanisms of silicon sputtering and cluster formation explained by atomic level simulations

Peter R. Barry,[a]* Patrick Philipp,[a] Tom Wirtz[a] and John Kieffer[b]

In low-energy secondary ion MS, collision cascades result in rare sputter events or unfavourably low sputter yields. To better identify the origin of emission products generated by low-energy ion impacts, we carried out molecular dynamics simulations of the underlying collision cascades, using a reactive force field that accounts for the dynamic breaking and forming of bonds. A detailed explanation of the cluster formation and ejection processes for atomic oxygen and also atomic silicon bombardment of Si (100) is given for comparison. Copyright © 2014 John Wiley & Sons, Ltd.

Keywords: simulation; silicon; clusters; oxygen; SIMS

Introduction

Because of its high sensitivity and dynamic range of elemental detection while requiring minimal sample preparation, secondary ion MS (SIMS) is a popular technique in the semiconductor industry for the profiling of dopants and impurities. Primary ion bombardment of a surface induces subsurface atomic mixing leading to complex responses in the form of ejection of surface matter at different rates[1,2] as a function of the chemical state of the sample,[3–7] variations in secondary ion yields[8,9] and in some cases surface roughening.[10,11] The process is further complicated, considering that a pre-equilibrium regime exists where the sputter rate and ion yields vary significantly,[12,13] thus rendering quantification at very shallow depths practically impossible. This drawback, in conjunction with the continued miniaturisation of electronic devices as well as the application of SIMS to organic matter,[14] has required depth profile resolutions of less than 0.5 nm/decade.[15] Such a requirement inevitably implies the reduction of the primary ion energy to the sub keV range, which has consequences such as reduced sputter/ejection of particles, oftentimes with yields <1. The resulting situation then is often one where depth profiling may become impractical. Mainly shallow subsurface implantation[16] of the primary ions, without desorption of secondary ions, is achieved as impact energies approach that of the threshold for sputter. Varying the incident angle while using reactive species such as oxygen[10,12,17] and caesium[18,19] has been attempted with varying degrees of success. Clearly, fundamental atomic level insights into the low energy (LE), sputter induced, collision cascade processes are needed.

Atomic level simulations in the form of binary collision approximation[20–27] and molecular dynamics (MD) simulation[28–33] are frequently used to explain such chaotic cascade phenomena while complementing experiments in related, problematic areas. For example, the mass distribution of detected cluster species can be the result of recombination of emission products into more stable clusters as opposed to representing actual ejected species.[34] Garrison *et al.*[35] have carried out MD simulations to clarify the range of internal energies experienced by ejected organic molecules upon keV bombardment. In another study on the bombardment of an organic layer on a metal substrate, Garrison *et al.*[36] describe two potential mechanisms by which molecules or their fragments may be lifted off of a substrate. The first occurs when a molecule maintaining multiple contact points with the substrate is cooperatively pushed upwards upon substrate perturbation by the primary species' imparted energy. The second mechanism involves vertically oriented surface chains or large fragments. The primary species thus colliding at the base or middle of the chain clips off a smaller fragment, which is then ejected. In Topics in Applied Physics 110 (Sputtering by Particle Bombardment),[37] a chapter by Urbassek, H.M., also discusses many proposed mechanisms of cluster formation ranging from the direct ejection of intact dimers and the recombination model to so-called push-stick events where a cascade atom colliding with a surface atom is ejected together with a surface atom in a bound state.

In regard of defect production in collision cascades, various simulation studies of amorphisation mechanisms and damage due to self-bombardment under different conditions have been reported in the literature. Nordlund *et al.*[38] have conducted detailed atomic scale simulations characterising the effect of crystal structure, atomic mass, melting temperature and other material properties on defect production. Their studies of silicon show that the open nature of the diamond crystal structure and slow damage regeneration due to covalent bonding facilitate damage production and the mixing caused by cascades. In a more recent article, Nord *et al.*[39] show that amorphisation of Si, Ge and GaAs occurs via a process somewhere in between a heterogeneous and homogeneous mechanism. In this context, Pinzon and Urbassek[31] show that total number of defects created and of

* *Correspondence to: Peter R. Barry, Science and Analysis of Materials Department, Centre de Recherche Public – Gabriel Lippmann, 41 Rue du Brill, L-4422 Belvaux, Luxembourg. E-mail: barry@lippmann.lu*

a *Science and Analysis of Materials Department, Centre de Recherche Public – Gabriel Lippmann, 41 Rue du Brill, L-4422, Belvaux, Luxembourg*

b *Department of Materials Science and Engineering, University of Michigan, Ann Arbor, Michigan, 48109-2136, USA*

relocated atoms depend only slightly on the incident polar angle (i.e. 30° or 60° in comparison with normal incidence).

In this work, the structural evolution of the sample subject to LE bombardment is characterised and correlated with the observed sputter behaviour. Thereafter, special attention is devoted to the mechanisms involving the formation and ejection of clusters at a low bombardment energy (250 eV). To this end, MD simulations are carried out to realistically describe the full range of atomic, dynamic behaviour within a solid resulting from the onset of collision cascades. A reactive force field that explicitly accounts for charge transfer during bond breaking and formation is employed.

Computational set-up/details and experimental details

The silicon diamond cubic structure (space group Fd3m at 25 °C, 1 atm)[40] is used as the initial starting configuration. MD simulations of oxygen bombardment of a symmetrically reconstructed Si (100) surface are carried out using a $43.88 \times 43.88 \times 81.45$ Å^3 silicon slab (7680 atoms). A second, separate symmetrically reconstructed Si (100) surface measuring $43.88 \times 43.88 \times 43.88$ Å^3 (4096 atoms) is bombarded with silicon atoms for comparison. A smaller Si surface is employed for Si bombardment of Si for computational cost savings as the interaction zone of Si bombardment of Si in this study is expected to be significantly shallower than that for O bombardment of Si. Whereas experimentally, silicon self-bombardment is not a commonly employed practice, simulation can be used to isolate and clarify specific effects, for example, the influence of atomic mass in this particular case. Note that, unlike in experiments, simulations allow one to distinguish between primary and secondary Si atoms without isotope substitution. All other simulation details between the types of simulations are identical. Two bombarding species (atomic oxygen and atomic silicon) with energy of 250 eV at an incident angle of 60° to the surface normal are separately used. Each impact location on the surface is randomly chosen. A small simulation time step of 0.05 fs is employed to account for the high velocity of the primary atom. The bombardment of the surface and ensuing collision cascades and/or ejection of atomic species are carried out for 1 ps. This period allows for sufficient dissipation of energy throughout the structure via the attenuation of the collision cascades and/or the ejection of surface atoms. This phase is simulated with constant number of atoms (*N*), at constant volume (*V*) and at constant energy (*E*), i.e. the *NVE* ensemble. After the completion of the *NVE* simulation phase, a different simulation ensemble is initiated at constant temperature (*T*), i.e. the *NVT* ensemble, and maintained for approximately 0.25 ps. This second phase consists of scaling the velocities of all atoms in the simulation such that the system's temperature, after having increased upon agitation of the atoms because of bombardment, is reduced to 300 K. This two-step process is repeated for a total of 111 atomic bombardments for both oxygen and silicon bombardment of silicon for a total simulation time of ~0.15 ns in each case.

The execution of 111 atomic bombardments within a time span of 0.15 ns results in a simulation flux rate higher than that in bombardment experiments (i.e. flux rates on the order of 10^{-3} to 10^{-6} particles per second). The MD technique samples phonon periods on the order of fs, resulting in total simulation times on the order of ns for nanometre size systems. As a result, the high simulation flux rate is a necessary compromise in the application of the MD technique to bombardment experiments. We adapted our system size in order to implement a dose of ~10^{14} atoms/cm^2. Given Si low degree of recrystallisation upon amorphisation, we reason that the approximate time between impacts and the total simulation time are reason sufficient to characterise damage and rearrangement of the impacted structure within the aforementioned constraints of the technique. Experiments under similar conditions involving oxygen bombardment at 250 eV of a silicon sample at an incidence angle of 60° with respect to the surface normal are carried out in our laboratory. The experimentally determined sputter yield is mentioned in the Results Section.

We used the potential by Kieffer *et al.*[41–45] to model the structure and dynamic properties of cristobalite silica and other silicon–oxygen systems. The potential incorporates a charge transfer term and adjusts angular constraints dynamically with change in atomic coordination. This potential has been shown to possess transferability between material systems, ranging from oxides[41,42] to organic compounds.[46] The reactive three-body potential includes a Coulomb term, a Born-Huggins-Mayer repulsive term as well as a three-body term:

$$\phi_i = q_i \sum_{j=1}^{N} \frac{q_j}{4\pi\varepsilon_0 r_{ij}} + \sum_{j=1}^{NC} C_{ij} e^{\left(\sigma_i+\sigma_j-r_{ij}\right)\cdot\rho_{ij}} + \sum_{j=1}^{NC-1}\sum_{k=j+1}^{NC}\left(\varphi_{ij}+\varphi_{ik}\right)\left(4e^{-\gamma_{ijk}\left(\overline{\theta}-\theta_{ijk}\right)^4}-3\right) \quad (1)$$

where ϕ_i is the potential energy of the particle, q_i is the charge, ε_0 is the dielectric constant of the vacuum and r_{ij} is the interatomic distance. Coulomb interactions are calculated by summing over *N* atoms up to the cut-off distance of the Ewald summation, whereas the other interactions sum over *NC* neighbours up to the cut-off distance of the Born-Huggins-Mayer term. The charge of each atom is given by equation $q_i = q_i^O - \sum_{j=1}^{NC}\delta_{ij}\zeta_{ij}$, where q_i^0 is the charge of the isolated atom and $\zeta_{ij} = \frac{1}{1+e^{b\left(r_{ij}-a\right)}}$ is the charge transfer function. Both, *a* and *b* are empirical parameters. Covalent bonding is modelled using the term $\left(\varphi_{ij}+\varphi_{ik}\right)\left(4e^{-\gamma_{ijk}\left(\overline{\theta}-\theta_{ijk}\right)4}-3\right)$, where $\varphi_{ij} = -C_{ij}\frac{\kappa_{ij}}{\eta_{ij}}\zeta_{ij}e^{\left(\lambda_{ij}-r_{ij}\right)\eta_{ij}}$ describes the attraction between two atoms, $\overline{\theta}$ is the equilibrium bond angle and θ_{ijk} is the angle formed by the bond vectors r_{ij} and r_{ik}. Furthermore, $C_{ij} = A_{ij}\left(1+\frac{z_i}{n_i}+\frac{z_j}{n_j}\right)$ where z_i is the valence and n_i is the maximum number of electrons in the outer shell of atom *i*. Coulomb interactions are calculated using the Ewald summation method. For the low impact energies studied in this paper, an interpolation to a high-energy potential such as the ZBL potential is not required. A more detailed description of the original force field can be found in the study of Huang and Kieffer.[43] Modifications to that potential as well as the optimisation of Si–O parameters are described in the study of Philipp *et al.*[47]

Results

As mentioned in the Computational Set-up/Details and Experimental Details Section, two separate silicon samples are bombarded individually with atomic oxygen and also atomic silicon at 250 eV. The bombardment process leads to the implantation of the primary atom in the silicon sample.

Figure 1 gives the implantation depth upon impact for energetic oxygen (Fig. 1(a)) and silicon atoms (Fig. 1(b)) on two

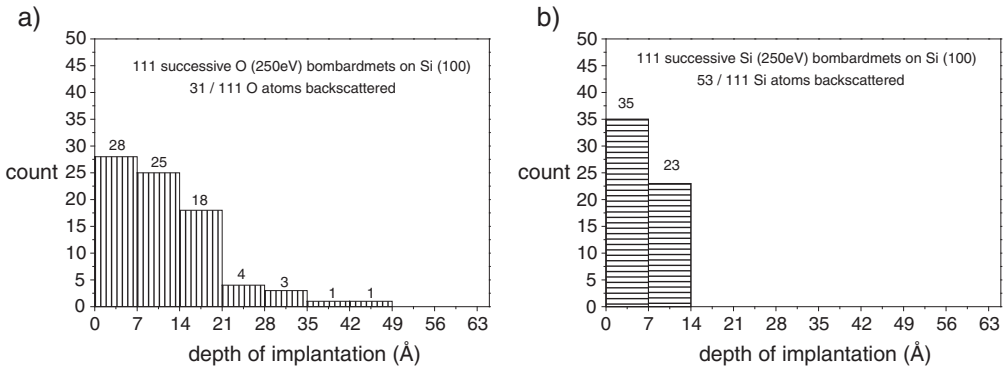

Figure 1. Implantation depth in Å beneath the plane of impact for (a) oxygen bombardment of silicon and (b) silicon bombardment of silicon.

separate Si (100) surfaces. A larger percentage (72%) of the bombarding oxygen atoms implant into the silicon surface compared with that for silicon bombardment (52%). For silicon bombardment, all implanted silicon atoms remain within the first 14 Å beneath the impact surface, which is in stark contrast to the case for oxygen bombardment. Quantitatively, ~48% of the 111 oxygen impacts remain within a depth of 14 Å beneath the surface, whereas for silicon impacts, the percentage is just slightly higher at 52%. Thus, at the depths of the subsurface region from which atoms are mostly likely ejected at such low impact energy, a roughly equal number of implantation species (be it oxygen or silicon) is achieved.

The bombardment and implantation of primary atom species undoubtedly modify the structure of the silicon surface. This structural change is captured by the pair correlation function illustrated in Fig. 2. After 101 consecutive bombardments, the pair correlation function is shown for the two separate bombardment cases to a depth range of approximately 21–30 Å beneath the surfaces impact plane. Both graphs (Fig. 2(a) and 2(b) for oxygen bombardment of silicon and silicon bombardment of silicon, respectively) illustrate a radial distribution function of short-range order, typical of that for amorphous silicon.[48] For the case of oxygen bombardment, there is a small peak at a distance of 1.76 Å, which is attributed to oxygen substitution in the silicon lattice.

To further explore the extent of structural change due to bombardment, the two bombarded silicon targets are analysed with respect to Si–Si bond length as a function of depth into the target from the plane of impact. Five adjacent zones, each 7 Å in thickness and ranging from the plane of impact to a maximum depth of 35 Å, are analysed. This range represents the widest region of physical, subsurface damage because of LE bombardment. The mean and median Si–Si bond lengths are practically identical (~1% difference). This trend holds as a function of depth beneath the plane of impact. Over a subsurface depth range of 0–35 Å, the average Si–Si bond length varies by a maximum of 2% from an overall average value of 2.37 (Table 1). The maximum average layer value of 2.39 Å is ~2% larger than the experimental value of 2.33 Å. A comparison of the two bombardment cases shows resulting average Si–Si bond lengths that are slightly lower for oxygen bombardment (2.36 Å) but with a significantly larger standard deviation compared with bombardment by silicon (i.e. average standard deviation over a depth range of 0–35 Å, Si ➔ 0.14, O ➔ 0.23).

For both bombardment cases, instances of two simultaneous atomic ejections or the ejection of Si–Si 'clusters' are examined more closely in terms of bond lengths before ejection. The average bond lengths of the ejected clusters are identical, with an average value of 2.37 Å and standard deviation of 0.10 and 0.08 as shown in the last two columns of Table 1.

Figure 3 illustrates the change in coordination of silicon atoms as a function of depth beneath the plane of impact after 29 and 111 consecutive impacts. In comparing Fig. 3(a) and 3(b) for oxygen bombardments of 29 and 111 impacts, respectively, one observes that over the depth range considered, the number of low-coordinated silicon atoms (i.e. onefold, twofold and threefold coordinated Si) increases noticeably at the expense of the fourfold coordinated Si atoms. Because of oxygen incorporation into the structure, a small fraction of the silicon atoms are fivefold coordinated. These are observed in Fig. 3(a) at depth ranges of 7–21 and 28–34 Å beneath the impact plane. In Fig. 3(b), this range spans 14–34 Å beneath the impact plane.

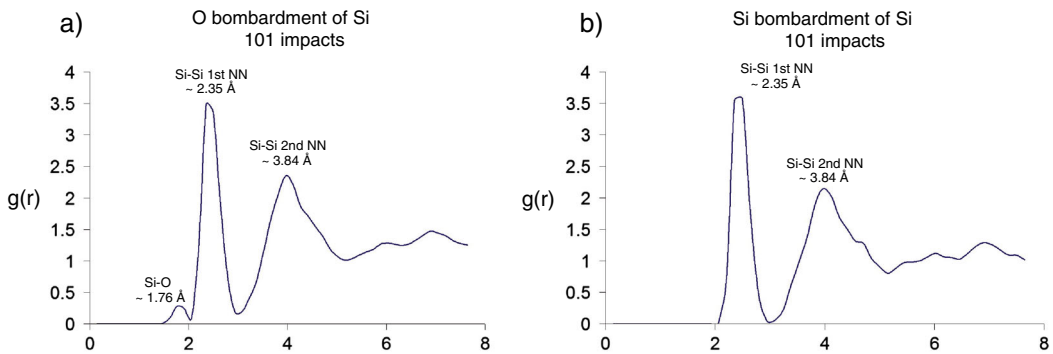

Figure 2. The pair correlation function of the silicon surface used in this study are shown after 101 consecutive bombardments of separate silicon surfaces by (a) oxygen and (b) silicon. The radial distribution function is calculated over a range of 21–30 Å beneath the plan of impact.

Table 1. Si–Si bond lengths as a function of depth beneath the impact surface for silicon (blue) and oxygen (red) bombardment and their respective standard deviations

	Si bombardment		O bombardment		Ejection site	
Depth (Å) beneath surface	Si–Si bond length (Å)	Standard deviation	Si–Si bond length (Å)	Standard deviation	O impacts Si–Si bond length	Si impacts Si–Si bond lengths
0–7	2.37	0.19	2.35	0.27	2.37 ± 0.10	2.37 ± 0.08
7–14	2.34	0.20	2.34	0.29		
14–21	2.38	0.16	2.35	0.24		
21–28	2.39	0.09	2.37	0.20		
28–35	2.37	0.06	2.37	0.14		

The last two columns on the right give the average bond lengths and standard deviations during the period of ejection for Si dimer species right before impact and subsequent ejection.

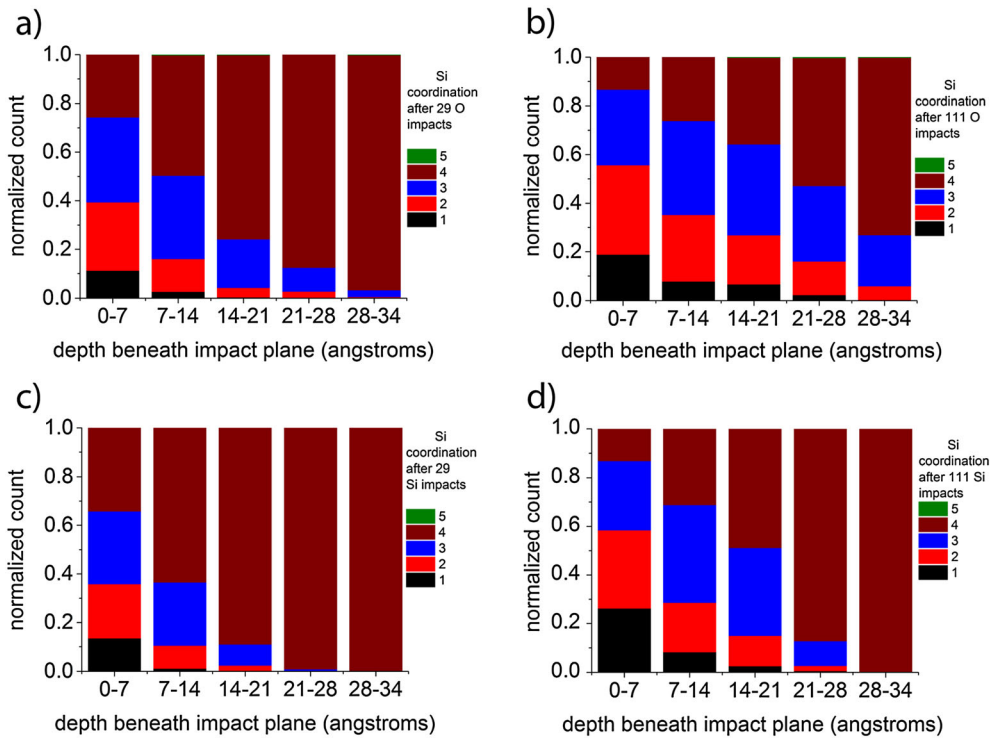

Figure 3. Coordination of silicon atoms at different stages of O and Si bombardment of a silicon surface.

A similar trend is observed in Fig. 3(c) and 3(d) for 29 and 111 Si impacts on the silicon surface. No fivefold silicon coordination is observed, unlike for oxygen bombardment. Also, at a depth range of 21–28 Å in Fig. 3(c), the silicon structure is almost completely fourfold coordinated. After 111 silicon impacts (Fig. 3(d)), at a depth range of 21–28 Å, the structure begins to resemble that of oxygen bombardment at the same depth range after 29 impacts. This is consistent with Fig. 1, where silicon is implanted at a much shallower range beneath the impact plane in comparison to oxygen bombardment. Hence, the damage zone due to silicon bombardment is smaller than that created by oxygen bombardment.

Silicon bombardment of a silicon surface at 250 eV gives a sputter yield superior to that of oxygen bombardment of a silicon surface under similar conditions. As Fig. 4 shows on the left panel, for approximately the first 25 successive bombardments (i.e. a little less than 2.0×10^{14} atoms/cm^2), the number of ejections for both cases is almost identical, and hence also, the instantaneous sputter yields (Fig. 4 right panel). Beyond a critical number of impacts, the number of ejections with successive bombardments begins to diverge for the two cases. At one point in the process, between 50 and 75 consecutive surface impacts, the instantaneous sputter yield for that of silicon bombardment attains a value more than twice that of oxygen.

After 111 successive impacts to their respective targets, bombardment by silicon yields 146 ejections for a sputter yield of ~1.32 and 82 ejections for a sputter yield of ~0.74 for oxygen bombardment. The sputter yield of 0.74 for oxygen bombardment is close to the experimental value of ~0.55, measured under similar experimental conditions (see Section on Computational Set-up/Details and Experimental Details) in our laboratory. Eckstein *et al.*[49] obtained higher sputter yields ranging from 0.9 to about 1.09 in employing a variety of repulsive potentials for silicon bombardment of silicon at 200 eV.

Journal of MASS SPECTROMETRY

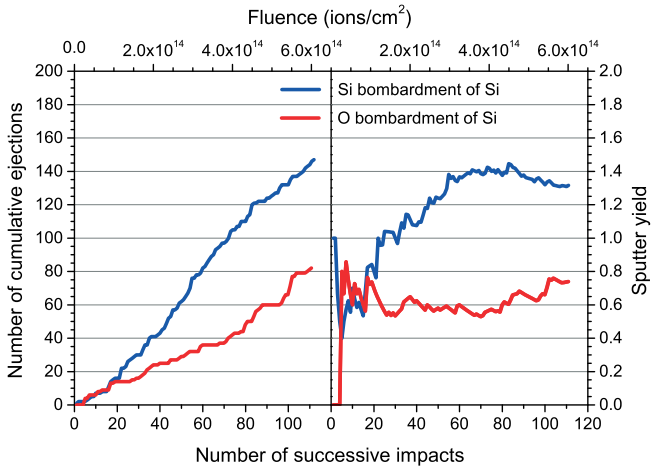

Figure 4. The cumulative number of sputtered atoms for Si bombardment of Si and O bombardment of Si with successive impacts plotted on the left panel and instantaneous sputter yield for the same data set on the right panel.

Ejection of particles and clusters

Table 2 shows the number of different ejected species as a result of two separate silicon targets being bombarded at 250 eV with single oxygen atoms and single silicon atoms, respectively. The dominant ejected specie for both oxygen and silicon bombardment of the surface is that of single silicon atoms (~79% of the ejected species). The second most favourable specie ejected is silicon dimers (15–18% of the ejected species). The other types of ejected species (i.e. Si–O and Si–Si–O for oxygen bombardment and Si–Si–Si for silicon bombardment) account for the minority cases.

The observed levels of cluster formations from our MD simulations results are consistent with their corresponding literature heat of formation values.[50] In other words, larger positively values of the calculated formation energy of the clusters imply a lesser frequency of cluster observance in our simulations. For silicon bombardment of silicon, the ejected species, in order of decreasing frequencies (as giving by Table 2) are Si, Si–Si and Si–Si–Si. Accordingly, the formation energies[50] are increasing in this order as it is more difficult to form Si–Si–Si on bombarding a silicon sample as opposed to Si, all things considered equal. The observed behaviour under oxygen bombardment of silicon is less obvious. As a comparison of their formation energies would reveal, Si–O and Si–Si–O species are energetically favourable than the Si cluster species; however, they are ejected to a comparably much lesser extent in this study. To understand this, it is necessary to consider the complete silicon–oxygen precursor sequence. As is common knowledge, oxygen has a strong affinity for silicon and readily forms a variety of glass compounds.[40,51] As previously mentioned, almost ¾ of the impacting primary oxygen atoms remain implanted within the silicon surface. Figure 9 highlights some of the resulting silicon–oxygen structures. As expected, with a valence of 2, oxygen forms an 'oxygen bridge' in silicon (i.e. Si–O–Si), thereby breaking up the tetrahedral silicon network. Other silicon–oxygen bond types formed include Si–O and Si–Si–O as transient small fragments within the structure; however, these cases are in the minority.

Table 2. The total count of ejected species at the end of the simulations after 111 consecutive bombardments

Primary ion	Si	Si–Si	Si–O	Si–Si–Si	Si–Si–O	Total number of bombardments
Oxygen	59	11	4	0	1	111
Silicon	95	22	0	4	0	111

Figure 1(a) illustrates that 80 of the 111 primary oxygen atoms with energy of 250 eV are implanted. Of these 80, only 28 are implanted at a depth of 7 Å beneath the plane of impact (i.e. depths from where atoms are most likely to be ejected from the surface). By comparison, at the end of the simulations, the silicon to oxygen ratio is ~24 : 1 at shallow depths near the impact plane. This is partly due to the timescale for the MD technique, which here, allows for primary atom fluence on the order of 10^{14} atoms/cm^2. Given this condition and the low impact energy of 250 eV, low sputter yields are observed for oxygen bombardment. This also affords fewer opportunities for sputter events to lead to cluster formation and ejection involving primary O atoms. Thus, single silicon atoms and small silicon clusters are favoured for ejection. We reason that in a situation of higher oxygen fluence, on the order of 10^{16} to 10^{17} atoms/cm^2, where a substantially larger number of oxygen atoms may be maintained at shallow depths in the near-impact subsurface region, a significantly larger fraction of ejected species would be present as small clusters comprising of O atoms.

Analysis and discussion of cluster sputter mechanisms

The most obvious explanation for the sputter behaviour observed from our MD simulations is based on the difference in mass between the bombarding silicon and oxygen. Interestingly, the ratio of the two sputter yields (1.32/ 0.74; Fig. 4) gives a factor of ~1.78, which is only 3% greater than the corresponding ratio of atomic masses. Oxygen has an atomic mass of 15.99 g/mol, whereas that of silicon is 28.086 g/mol, thus approximately 1.75 times more massive than oxygen. At an impacting energy of 250 eV, the oxygen atom has a linear momentum that is ~3/4 that of a silicon atom with identical impacting energy. This implies that under these physical conditions (and putting aside for the moment arguments of primary atom chemical effects), silicon impacts induce more surface damage and hence sputter more strongly compared with oxygen impacts. Indeed, this is the case. Furthermore, given the inherently low simulation fluence (as mentioned in the Results Section regarding the shallow subsurface silicon to oxygen ratio), a silicon oxide layer is not observed, thus limiting potential chemical effects on both sputter yields and ejection of oxide clusters.

Figure 5 supports the hypothesis of enhanced surface damage with silicon impacts in depicting the cumulative ejection frequency of Si–Si clusters as a function of consecutive bombardment for the two cases. It is interesting to note that for oxygen bombardment of silicon (the red curve), the rate of Si–Si dimer ejection may be divided into two regimes. The crossover between regimes is at about the 80th consecutive bombardment (i.e. fluence of ~4.4×10^{14} ions/cm^2). For silicon bombardment of silicon (blue curve), only a single regime is observed, as the Si–Si dimer sputter rate remains essentially constant. For oxygen bombardment, the difference in the two phases concerns the ejection rates, i.e. the reciprocal of the time intervals between cluster ejection events. The initial regime is marked by longer

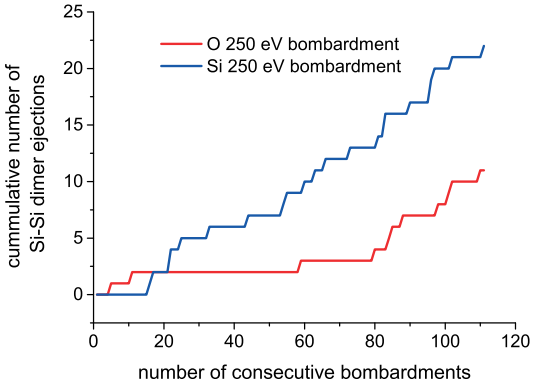

Figure 5. Evolution of Si dimer ejection for O and Si bombardments.

periods between cluster ejection events, compared with shorter periods during the latter regime, which is reflected in a significant increase in the slope. The sputter yields (i.e. all ejected species included) over the initial and latter phases are 0.57 and 1.31, respectively. We surmise that, given its inferior mass, oxygen bombardment requires a larger number of impacts to attain corresponding amounts of surface damage as compared with silicon impacts. We further reason that the extent of the surface damage is directly related to rate of sputter. The rate of sputter is practically identical in Fig. 5 after approximately 80 consecutive impacts.

As mentioned previously, the size and mass of the bombarding species play an important role in the sputter process and hence the evolution of damage accumulation in the irradiated area and surface roughness. In comparing the simulation snapshots for silicon and oxygen bombardment, one can follow the differences in the evolution of the surface roughness. In Fig. 6, by visually comparing the surface after 22 impacts to that after 83 impacts, it is clear that surface roughness increases upon continued bombardment. In Fig. 7 where the difference in the number of silicon impacts is smaller, (a difference of 61 impacts in Fig. 6 compared with 23 in Fig. 7), it is still evident that more fragments protrude vertically from the surface after 78 impacts in comparison to that after 55 impacts. Figure 8 shows the beginning phase of oxygen bombardment on silicon (i.e. after only 5 and 11 impacts). Here, the surface roughness is almost at the level of atomic, lattice corrugations expect for a few protrusions demonstrating the ejection process. In transitioning to Fig. 9 at considerably higher number of oxygen impacts (i.e. 101), the bombardment surface is evidently much more corrugated and dominated by the presence of small protruding fragments as for silicon bombardment.

Placing a reference plane perpendicular to the *z*-axis, along the surface, starting at the topmost protruding atom and moving it downwards incrementally at fixed Δz, beneath the plane of impact, each time keeping a cumulative total of the number of atoms above the reference plane, on obtains a quantitative *z*-dependent profile of the surface roughness. This procedure is used to generate the graphs of Fig. 10 depicting the cumulative number of atoms above the reference line as a function of depth beneath the impact plane. A Δz increment of 0.5 Å is used. By this method, the rougher surfaces initially demonstrate (at shallow subsurface depths) a smaller slope, whereas the more smooth surfaces have a somewhat steeper slope. At large enough depths beneath the plane of impact, the slopes of the graphs should increase at similar, constant rates as the additional atoms added above the reference line are no longer surface atoms but those of the amorphous or crystalline bulk.

Figure 10 corroborates the surface roughness conclusions on the basis of visual inspections of Figs. 6–9. Figure 10(a) and 10 (b) shows the cumulative atom count above the sliding reference line to a depth of 25 Å. The slopes for all of the graphs are practically identical at distances beyond ~7 Å beneath the plane of

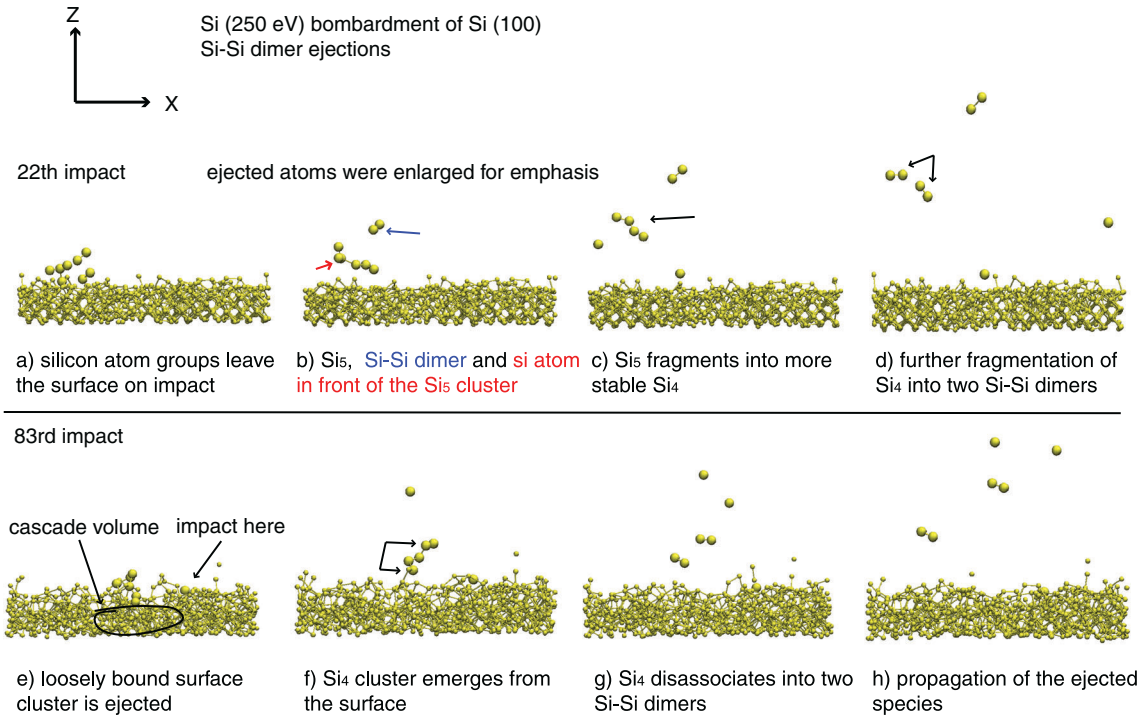

Figure 6. Two groups of simulation snapshots showing the progression from the ejection of silicon fragments upon bombardment. Periodic boundary conditions are employed in the *x* and *y* directions.

Journal of MASS SPECTROMETRY

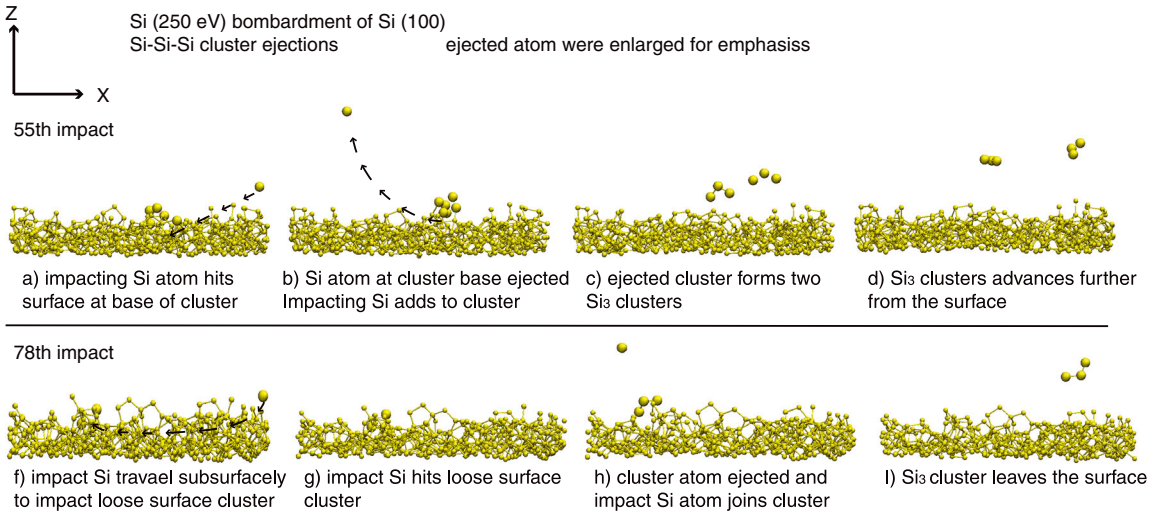

Figure 7. Two groups of simulation snapshots of silicon bombardment of silicon at impact numbers 55 and 78 depicting the ejection of Si–Si–Si fragments. Periodic boundary conditions are employed in the *x* and *y* directions. The arrows indicate atomic trajectories.

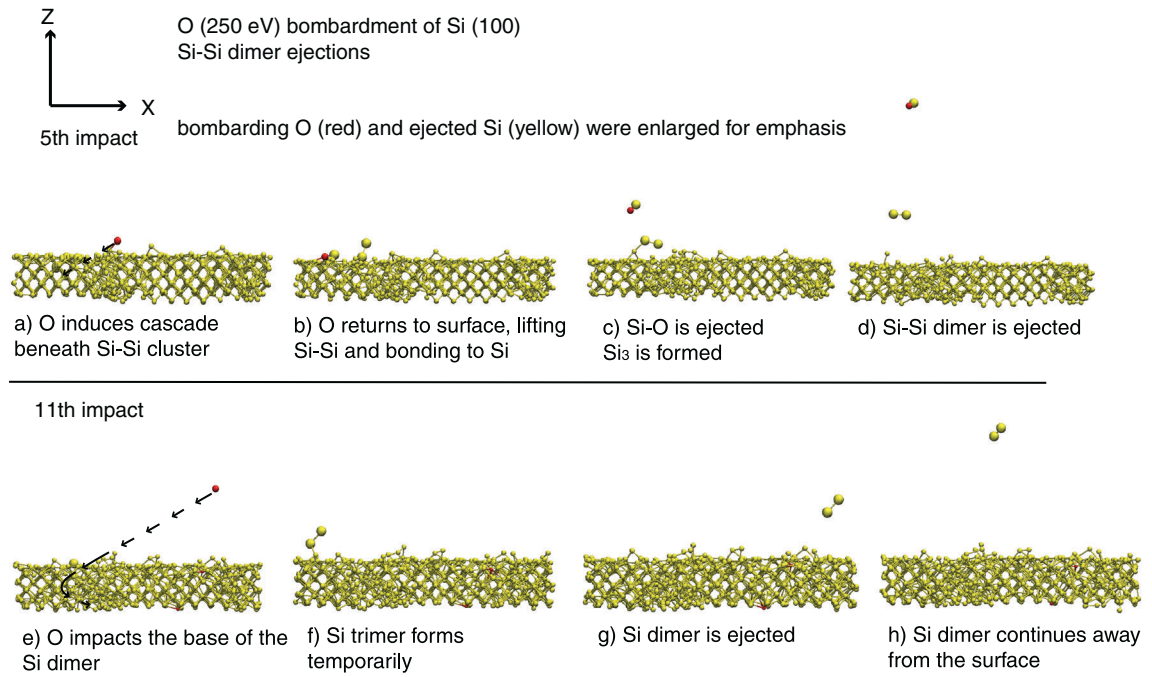

Figure 8. Oxygen bombardment of Si (100) surface where dimers are ejected. Periodic boundary conditions are employed in the *x* and *y* directions of the surface. In (a) the Si atoms from which the dimers are to be formed are initially 3.25 Å apart.

impact. Figure 10(c) and 10(d) examines the shallow subsurface region in the range of 0–7 Å, as this region is dominated by the surface atoms.

The black, stepwise curve represents the pristine crystalline silicon surface prior to simulation. The horizontal segments in these steps correspond to open spaces between crystal planes. The lengths of all vertical segments are identical. Figure 10(c) shows that with increasing number of silicon impacts, the surface roughness increases, as is evident by decreasing slopes (i.e. the numbers next to each segment of the curves) in the range of 0–4.5 Å. In Fig. 10(d), a similar behaviour is observed for oxygen impacts, except that, here, the dynamic evolution of the surface roughness is captured, because after the 78th oxygen impact, the surface roughness is higher than at the 101st impact. A similar behaviour (not shown in graphs) in surface roughness is also captured for silicon bombardment by comparing data after 83rd and 101st impacts, where the latter shows lower surface roughness (because of removal of protruding, loosely bound surface clusters) than the former. Regardless of the natural fluctuations of the surface roughness with extended number of impacts, it is clear that the surface becomes more heavily damaged with increasing impacts, and this accumulated surface damage fosters the ejection of various species as depicted in Table 2 and Fig. 5.

The ejection of small clusters in this study involves primarily one of two mechanisms. In one mechanism, small clusters form just above the impacted surface site immediately after ejection

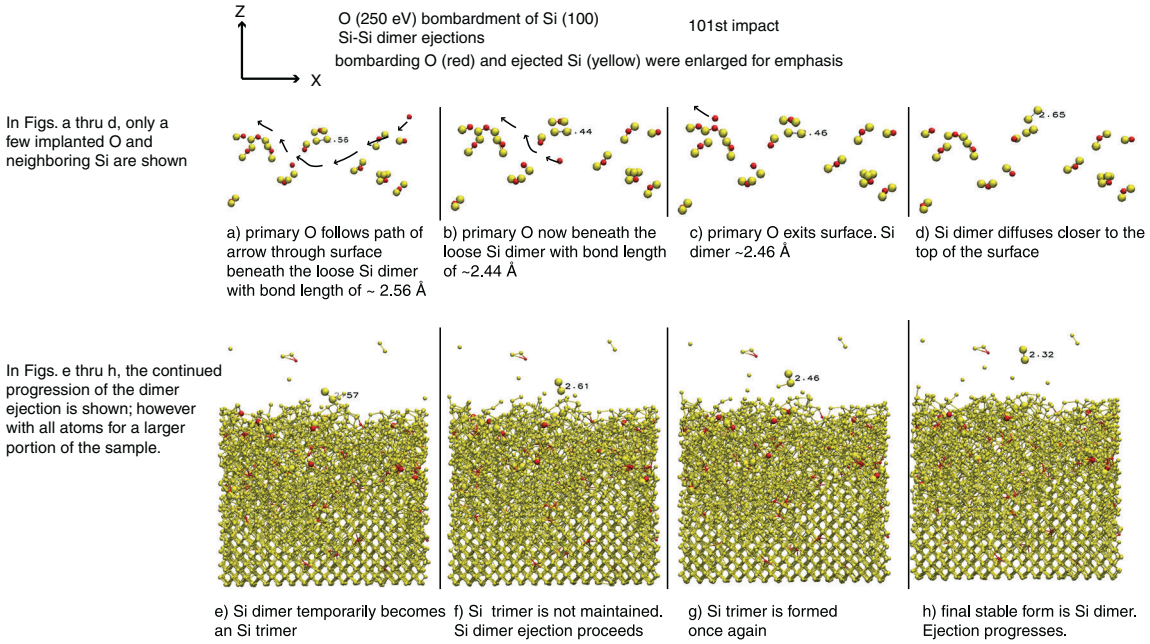

Figure 9. Oxygen bombardment of Si (100) surface where Si–Si dimers are ejected. Periodic boundary conditions are employed in the *x* and *y* directions of the surface. The instantaneous dimer bond length is noted in some of the snapshots.

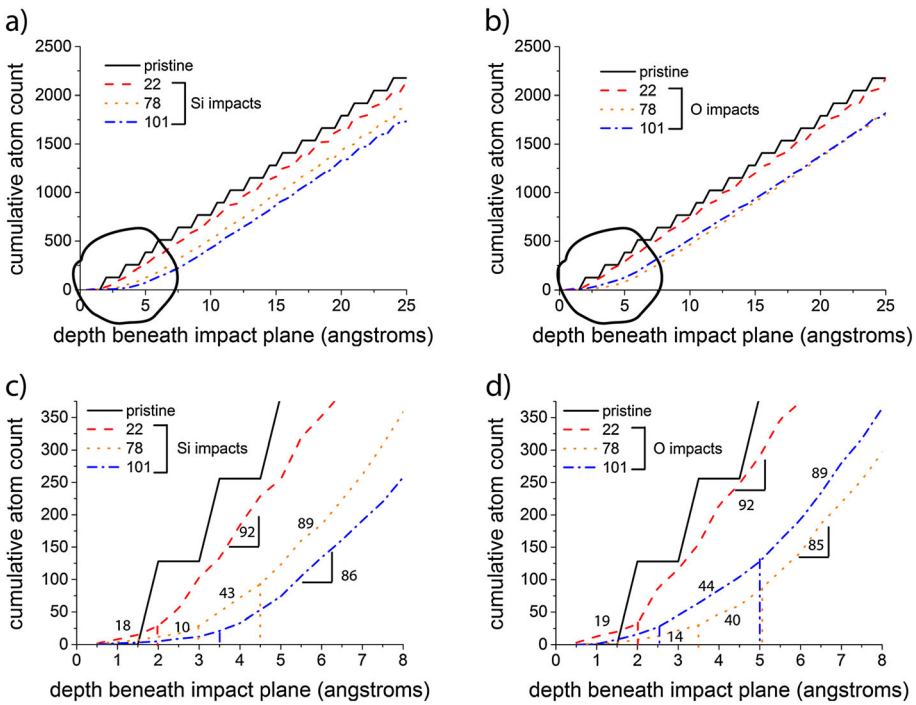

Figure 10. Cumulative total of atoms from the plane of impact to within the surface at successive, increasing intervals of $\Delta z = 0.5$. Curves are given after chosen number of consecutive impacts. The numbers adjacent to the curves denote their slopes at various intervals (maximum of three intervals given per curve) are given on the basis of linear fits for segments of each curve.

of atomic entities. This mechanism is a characteristic of the recombination model discussed in the Introduction Section.[37] For this mechanism, the sputtered atoms are not directly attached prior to impact but instead are ejected from the same local area of the surface. Upon ejection, and owing to initial trajectories that intersect, these individually ejected species quickly form small clusters, which may or may not maintain their structural integrity as they slowly (in comparison to most cases of single species ejection) move together and away from the surface of impact. An example is given for oxygen bombardment of silicon in Fig. 8(e): after the 11th impact the silicon atoms that eventually form a dimer were initially 3.25 Å apart.

In the second mechanism we observed, the cluster is 'lifted' off of the surface because of perturbations from bombardment and is similar to the mechanisms described by Garrison *et al.*[36] In some cases, direct ejection of dimers is observed. In Fig. 6(e–h),

Journal of MASS SPECTROMETRY

after the 83rd impact, an initially larger cluster is lifted off of the surface by a Si atom (indicated with the arrow) impacting the surface, a few angstroms from the location at which the cluster is to be ejected. As a result of subsurface collision cascades, the two cluster groups (consisting of a silicon trimer and a dimer) are lifted off of the surface (Fig. 6(e) and 6(f)). In Fig. 6(g) and 6(h), the dissociation of the trimer group leads to the ultimate ejection of two dimer groups. Figure 7(a–d) also shows the trajectory (with arrows) of the 55th impacting silicon atom, which strikes the base of the surface cluster and thereby 'lifting' a cluster of six (6) silicon atoms (later in Fig. 7(c) to be dissociated into two distinct trimer groups) off of the surface. Yet, in Fig. 7(f), upon the 78th silicon impact at grazing incident angle (indicated by the curved arrows) travels just below the surface and makes contact with a surface Si trimer from the side along the *x*-axis and 'lifts' it off the surface.

In some cases, a combination of the two mechanisms works cooperatively to form the same cluster. For example, Fig. 9(a) depicts a silicon dimer on the surface with a bond length of 2.56 Å prior to the 101st O impact onto Si (100) at 250 eV. After impact, this cluster gains enough energy to be ejected from the surface as is noted in Fig. 9(e) with a bond length of 2.57 Å. In Fig. 9(g), the dimer temporarily forms a silicon trimer in attaching to another ejected lone silicon atom. Figure 9(h) shows that the trimer is short-lived; it disintegrates into the original dimer and the most recently acquired lone silicon atom. Yet, another example of the combined mechanism is given in Fig. 6 upon the 22nd impact of silicon on Si (100). Figure 6(a) shows a group of loosely bounded atoms, consisting of at least three Si dimer groups that are lifted off the surface. Figure 6(b) shows two groups, a Si_5 group and a Si dimer group, formed as a result of silicon recombination above the surface after ejection. The end result, however, is the fragmentation of the cluster into smaller, more stable clusters as is demonstrated by Fig. 6(c) and 6(d). It is important to note that the mechanisms describe mainly the ejection of clusters with two to four atoms are quite rare events and that most sputter events involve the emission of single atoms.

Conclusions

Molecular dynamics simulations have shown and described in detail, atomic process of small cluster formation during LE-SIMS of a silicon surface, comparing bombardment by atomic oxygen and atomic silicon. The two primary ejection mechanisms are (1) Cluster formation from individual atoms only a few angstroms above the impacted surface immediately after ejection, and (2) The lifting off of loosely bounded fragments resting on the damaged surface. On the basis of the findings for the majority of the observed cases herein, we conclude that many of the larger clusters (i.e. Si_3 and greater) resulting from the described mechanisms fragment during ejection from the surface to form more stable, smaller Si dimers. Bombardment of silicon by atomic silicon exhibits a sputter yield superior to bombardment by atomic oxygen when both have impact energies of 250 eV. The sputter yield ratio coincides almost precisely with the ratio of atomic masses. In both cases, atomic silicon is the dominant ejected species. Cluster ejections increases during the course of bombardment, owing to a more pronounced surface roughness and accumulated subsurface damage. The description and explanations provided in this may give additional insights to experimentalists regarding atomic level processes of collision cascades of silicon, the ensuing damage and ejection of clusters. These ideas may in turn aid in the formulation, construction and execution of future silicon SIMS experiments.

Acknowledgements

This work has been supported by the National Research Fund, Luxembourg (FNR-MAT-07-01) and the US National Science Foundation (NSF-DMR 0806867).

References

[1] P.A.W. van der Heide, M.S. Lima, S.S. Perry, J. Bennett. *Appl. Surf. Sci.* **2003**, *203*, II.
[2] P.A.W. van der Heide, F.V. Azzarello. *Surf. Sci.* **2003**, *531*, L369–L377.
[3] P. Williams. *Surf. Sci.* **1979**, *90*, 588–634.
[4] P. Williams. *Appl. Surf. Sci.* **1982**, *13*, 241–259.
[5] K. Wittmaack. *Surf. Sci.* **1983**, *126*, 573.
[6] T. Wirtz, H.N. Migeon. *Surf. Sci.* **2004**, *557*, 57–72.
[7] P. Philipp, T. Wirtz, H.N. Migeon, H. Scherrer. *Int. J. Mass Spectrom.* **2006**, *253*, 71–78.
[8] C. Mansilla, T. Wirtz, C. Verdeil. *Nucl. Instrum. Methods Phys. Res. B* **2009**, *267*, 2589–2591.
[9] P.A.W. van der Heide, M.S. Lim, S.S. Perry, J. Bennett. *Nucl. Instrum. Methods Phys. Res. B* **2003**, *201*, 413–425.
[10] Z.X. Jiang, P.F.A. Alkemade. *Surf. Interface Anal.* **1997**, *25*, 817.
[11] C. Mansilla, P. Philipp, T. Wirtz. *Nucl. Instrum. Methods Phys. Res. B* **2011**, *269*, 905–908.
[12] K. Wittmaack. *Philos. T. R. Soc. A* **1996**, *354*, 2731–2764.
[13] M.G. Dowsett. *Appl. Surf. Sci.* **2003**, *203–204*, 5.
[14] L. Houssiau, B. Douhard, N. Mine. *Appl. Surf. Sci.* **2008**, *255*, 970–972.
[15] B. Berghmans, W. Vandervorst. *J. Appl. Phys.* **2009**, *106*, 033509. http://dx.doi.org/10.1063/1.3190526
[16] W. Vandervorst, T. Janssens, C. Huyghebaert, B. Berghmans. *Appl. Surf. Sci.* **2008**, *255*, 1206–1214.
[17] P.F.A. Alkemade, Z.X. Jiang, C.C.G. Visser, S. Radelaar, W.M. Arnoldbik, J. Vac. *Sci. Technol. B* **1998**, *16*, 373–376.
[18] Y. Kataoka, K. Yamazaki, M. Shigeno, Y. Tada, K. Wittmaack. *Appl. Surf. Sci.* **2003**, *203–204*, 43–47.
[19] Y. Kataoka, M. Shigeno, Y. Tada, K. Wittmaack. *Appl. Surf. Sci.* **2003**, *203*, 329–334.
[20] J.P. Biersack, L.G. Haggmark. *Nucl. Instrum. Methods* **1980**, *174*, 257.
[21] W. Eckstein. *Nucl. Instrum. Methods Phys. Res. B* **2000**, *171*, 435.
[22] W. Eckstein. *Nucl. Instrum. Methods Phys. Res. B* **1987**, *18*, 344.
[23] W. Moller, W. Eckstein. *Nucl. Instrum. Methods Phys. Res. B* **1984**, *230*, 814–818.
[24] V.I. Shulga, W. Eckstein. *Nucl. Instrum. Methods Phys. Res. B* **1998**, *145*, 492.
[25] V.A. Ignatova, W. Moller, T. Conard, W. Vandervorst, R. Gijbels. *Appl. Phys. A-Matter* **2005**, *81*, 71–77.
[26] V.A. Ignatova, T. Conard, W. Moller, W. Vandervorst, R. Gijbels. *Appl. Surf. Sci.* **2004**, *231*, 603–608.
[27] T. Yoneda, K. Kajiyama, F. Tohjou, Y. Yoshioka, A. Ikeda, Y. Kisaka, T. Nishimura, Y. Kido. *Jpn. J. Appl. Phys. 1* **1997**, *36*, 7323–7328.
[28] I. Koponen, M. Hautala, O.P. Sievänen. *Nucl. Instrum. Methods Phys. Res. B* **1997**, *127–128*, 230–234.
[29] K. Gärtner, B. Weber. *Nucl. Instrum. Methods Phys. Res. B* **2001**, *180*, 274.
[30] R. Smith, D.E. Harrison, B.J. Garrison. *Phys. Rev. B* **1989**, *40*(1), 93.
[31] R. Pinzon, H.M. Urbassek. *Phys. Rev. B* **2001**, *63*, 195319.
[32] A. Duvenbeck, B. Weidtmann, A. Wucher. *J. Phys. Chem. C* **2010**, *114*, 5715–5720.
[33] K. Vörtler, K. Nordlund, J. Phys. *Chem. C* **2010**, *114*, 5382–5390.
[34] Behrisch and Rainer. Sputtering by particle bombardment 3, characteristics of sputtered particles, technical applications, Springer, Berlin [etc.] **1991**.
[35] B.J. Garrison, Z. Postawa, K.E. Ryan, J.C. Vickerman, R.P. Webb, N. Winograd. *Anal. Chem.* **2009**, *81*, 2260–2267.
[36] B.J. Garrison, A. Delcorte, K.D. Krantzman. *Acc. Chem. Res.* **2000**, *33*, 69–77.
[37] R. Behrisch, W. Eckstein. Sputtering by Particle Bombardment: Experiments and Computer Calculations from Threshold to MeV Energies, Springer: Berlin; New York, **2007**.
[38] K. Nordlund, M. Ghaly, R.S. Averback, M. Caturla, T.D. de la Rubia, J. Tarus. *Phys. Rev. B* **1998**, *57*(13), 7556.

[39] J. Nord, K. Nordlund, J. Keinonen. *Phys. Rev. B* **2002**, *65*, 165329.
[40] Chemical Rubber Company (Cleveland, Ohio), R. D. Lide. CRC Handbook of Chemistry and Physics: 1994–1995; A Ready-Reference Book of Chemical and Physical Data. CRC Press: Boca Raton, u.a. **1994**.
[41] L.P. Huang, M. Durandurdu, J. Kieffer. *J. Phys. Chem. C* **2007**, *111*, 13712–13720.
[42] L.P. Huang, M. Durandurdu, J. Kieffer. *Nat. Mater.* **2006**, *5*, 977–981.
[43] L.P. Huang, J. Kieffer. *J. Chem. Phys.* **2003**, *118*, 1487–1498.
[44] L.P. Huang, J. Kieffer. *Phys. Rev. B* **2004**, *69*, 224203.
[45] L.P. Huang, J. Kieffer. *Phys. Rev. B* **2004**, *69*, 224204.
[46] J.H. Zhou, J. Kieffer, J. Phys. *Chem. C* **2008**, *112*, 3473–3481.
[47] P. Philipp, L. Briquet, T. Wirtz, J. Kieffer. *Nucl. Instrum. Methods Phys. Res. B* **2011**, *269*, 1555–1558.
[48] S. Dalgic, L.E. Gonzalez, S. Baer, M. Silbert. *Physica B* **2002**, *324*, 292–304.
[49] Eckstein, W., Hackel, S., Heinemann, D., B. Fricke. *Z. Phys. D. Atom. Mol. Cl.* **1992**, *24*, 171–176.
[50] N.M. Tam, M.T. Nguyen. *Chem. Phys. Lett.* **2013**, *584*, 147–154.
[51] D. R. Askeland, P. P. Fulay. The Science and Engineering of Materials. Thomson Brooks/Cole: Pacific Grove, CA, **2003**.